This is a peer-reviewed, author's accepted manuscript of the following conference procedings output:
Chen, C., Tavakkolnia, I., Soltani, M. D., Safari, M., & Haas, H. (2020). Hybrid multiplexing in OFDM-based VLC systems.
In 2020 IEEE Wireless Communications and Networking Conference (WCNC) (pp. 1-6). [9120825]
(Proceedings of the IEEE Wireless Communications and Networking Conference). IEEE. https://doi.org/10.1109/WCNC45663.2020.9120825

Hybrid multiplexing in OFDM-based VLC systems

Cheng Chen, Iman Tavakkolnia, Mohammad Dehghani Soltani, Majid Safari and Harald Haas
School of Engineering, Institute for Digital Communications, LiFi R&D Centre, The University of Edinburgh
E-mail:{cheng.chen, i.tavakkolnia, m.dehghani, majid.safari, h.haas}@ed.ac.uk

***Abstract*—In conventional visible light communication (VLC) systems with multiple light-emitting diodes (LEDs) and multiple photodiodes (PDs), high data rate transmission with limited modulation bandwidth can be achieved via spatial multiplexing (SMP) or wavelength division multiplexing (WDM). However, the number of multiplexing channels is limited by the strong spatial correlation in SMP and by the inter-colour crosstalk in WDM. In this paper, we propose a multiple-input multiple-output (MIMO) hybrid multiplexing (HMP) VLC system which avoids the disadvantages of SMP / WDM and explores the degrees-of-freedom (DoFs) in space and wavelength domains jointly. With appropriate system configuration, a MIMO channel matrix with a better channel condition in HMP can be obtained. Eventually, it is able to increase the number of multiplexing channels and support higher data rate transmission.**

***Index Terms*—Optical wireless communication, multiple input multiple output, spatial multiplexing, wavelength division multiplexing, orthogonal frequency division multiplexing.**

I. Introductions

For future wireless communication systems, a very high data rate for a single user is essential for many applications such as virtual reality, cloud-based system and ultra high definition video streaming. It has been shown that visible light communication (VLC)-based systems such as Light-Fidelity (LiFi) are able to effectively offload a huge amount of data traffic [1]. To increase the data rate of VLC systems, orthogonal frequency division multiplexing (OFDM) has been considered and experimentally validated [2]. However, this high data rate relies on a wide modulation bandwidth and high speed front-ends. In order to further increase the data rate with limited bandwidth, other multiplexing techniques have to be used. Sptial multiplexing (SMP) in a multiple-input multiple-output (MIMO) system has been considered in a number of studies [3]. In a VLC system, using intensity modulation with direct detection (IM/DD) without the effect of small-scale fading, it is challenging to obtain a full rank MIMO channel matrix. This significantly limits the number of independent multiplexing channels in SMP. Wavelength division multiplexing (WDM) is another promising technique to transmit multiple data streams in parallel. However, wide spectrum light-emitting diodes (LEDs) are typically used in VLC systems and the inter-colour crosstalk becomes severe when the number of wavelength divisions increases [4]. In addition, the passband of a thin-film optical filter shifts to shorter wavelengths when the light arrives at the optical filter with a non-zero incident angle [5]. These factors limit the data rate that can be achieved by WDM.

In order to further improve the peak data rate of a single VLC link with limited optical power and modulation bandwidth, it is intuitive to consider the combination of SMP and WDM. Multi-colour LEDs have been employed in a MIMO VLC system to improve the data rate in [6]. The authors focus on the optimal linear precoding design. However, the authors did not provide any result about the gain by including multi-colour LEDs and many practical issues, such as receiver size and optical filter passband shift, were neglected. A concept of colour-MIMO has been considered to use the MIMO signal processing techniques to improve the performance of WDM systems in [5]. However, the colour-MIMO system does not explore any degree-of-freedom (DoF) in space domain (SD). In the context of VLC, the DoFs in SD and wavelength domain (WD) are non-orthogonal. When applying SMP, differences in incident angles and received signal power are preferred in order to obtain a well-conditioned channel matrix, but this causes issues such as signal power loss and optical filter passband shifts. On the other hand, WDM requires more optical elements to be installed, which takes extra space. Especially for the mobile user device with limited surface area, the space resources for the purposes of WDM can no longer be used for SMP. In order to avoid the disadvantages of SMP and WDM, in this paper, we propose a MIMO-VLC multiplexing system that uses the DoFs in SD and WD jointly, which is named hybrid multiplexing (HMP). By using this method, the introduction of DoF in WD helps to decorrelate the channels those are difficult to be separated in SD. Additionally, the precoding and post-processing counterparts are able to mitigate the crosstalk between wavelength divided channels. In order to include the characteristics in both SD and WD into the HMP system, we establish a framework of a MIMO-OFDM system model based on a series of space and wavelength dependent parameters. The signal processing techniques designed for SMP systems can be adopted directly. Then, we show that by choosing appropriate configurations to space and wavelength dependent parameters, the number of multiplexing channels in HMP can be significantly increased and higher data rate can be supported.

The remainder of this paper is organised as follows. In Sections II and III, SMP and WDM techniques are reviewed respectively, and their limitations are explained by simulations. In Section IV, HMP is proposed and described in detail. The simulation results are presented in Section V. Finally, the conclusions are provided in Section VI.

II. Spatial multiplexing

Firstly, we consider a general singular value decomposition (SVD)-based SMP system using a MIMO-OFDM model, as

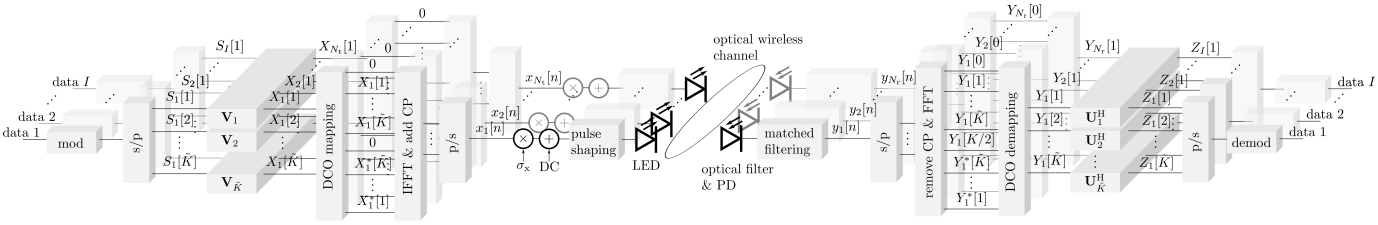

Fig. 1. The block diagram of a SVD-based VLC multiplexing system using a MIMO-OFDM model.

shown in Fig. 1. By using OFDM, a frequency-selective channel is sliced into K independent narrowband flat subchannels in frequency domain (FD). Note that the number of subcarriers carrying information bits is $\tilde{K} = K/2 - 1$. The signal transmission between N_{t} LEDs and N_{r} photodiodes (PDs) on kth subcarrier can be modelled by $\mathbf{Y}_k = \mathbf{H}_k\mathbf{X}_k + \mathbf{W}_k$ where $\mathbf{Y}_k \in \mathbb{C}^{N_{\mathrm{r}}\times 1}$ is the received signal vector, $\mathbf{W}_k \in \mathbb{C}^{N_{\mathrm{r}}\times 1}$ is the received noise samples vector, $\mathbf{X}_k \in \mathbb{C}^{N_{\mathrm{t}}\times 1}$ is the transmitted signal vector and $\mathbf{H}_k \in \mathbb{C}^{N_{\mathrm{r}}\times N_{\mathrm{t}}}$ is the MIMO matrix [3]. We apply SVD to the channel matrix: $\mathbf{H}_k = \mathbf{U}_k\mathbf{\Lambda}_k\mathbf{V}_k^{\mathrm{H}}$, where $(\cdot)^{\mathrm{H}}$ refers to the Hermitian transpose operation, $\mathbf{U}_k \in \mathbb{C}^{N_{\mathrm{r}}\times N_{\mathrm{r}}}$ and $\mathbf{V}_k \in \mathbb{C}^{N_{\mathrm{t}}\times N_{\mathrm{t}}}$ are unitary matrices. $\mathbf{\Lambda}_k \in \mathbb{R}^{N_{\mathrm{r}}\times N_{\mathrm{t}}}$ is a rectangular matrix with $I = \min(N_{\mathrm{t}}, N_{\mathrm{r}})$ non-zero entries on the diagonal corresponding to I eigen-subchannels. These entries are the square-root of channel matrix singular values. The unitary matrices $\mathbf{V}_k$ and $\mathbf{U}_k^{\mathrm{H}}$ are used as a precoder and a post-decoder, respectively. Then we have $\mathbf{X}_k = \mathbf{V}_k\mathbf{S}_k$ where $\mathbf{S}_k \in \mathbb{C}^{N_{\mathrm{t}}\times 1}$ is the modulated quadrature amplitude modulation (QAM) or on-off keying (OOK) symbols with a variance of σ_{s}^2 and non-zero entries as the first I elements. The symbols after post-processing is: $\mathbf{Z}_k = \mathbf{U}_k^{\mathrm{H}}\mathbf{Y}_k = \mathbf{\Lambda}_k\mathbf{S}_k + \mathbf{U}_k^{\mathrm{H}}\mathbf{W}_k$ The noise is attributed to the receiver thermal noise, shot noise from LEDs and background light. Without loss of generality, the noise variances on each receiver are defined separately as $\sigma_{\mathrm{w},n_{\mathrm{r}}}^2$. Thus, the signal-to-noise ratio (SNR) on the kth subcarrier of the ith eigen-subchannel can be written as:

$$\gamma_i[k] = \sigma_{\mathrm{s}}^2 \left[\mathbf{\Lambda}_k\right]_{i,i}^2 \left(\sum_{n_{\mathrm{r}}=1}^{N_{\mathrm{r}}} \sigma_{\mathrm{w},n_{\mathrm{r}}}^2 \left|\left[\mathbf{U}_k\right]_{n_{\mathrm{r}},i}\right|^2 \right)^{-1}, \qquad (1)$$

where $\left[\mathbf{M}\right]_{n_1,n_2}$ is the (n_1, n_2)-th element of a matrix $\mathbf{M}$. This shows that the SNRs are strongly related to the matrix $\mathbf{\Lambda}_k$, which is determined by the characteristics of $\mathbf{H}_k$. In conventional studies of MIMO in VLC, the entries of $\mathbf{H}_k$ are proportional to and different only in the term of optical wireless channel transfer function for a different pair of LED and PD: $\left[\mathbf{H}_k\right]_{n_{\mathrm{r}},n_{\mathrm{t}}} \propto H_{n_{\mathrm{r}},n_{\mathrm{t}}}^{\mathrm{ow}}\left(\frac{k}{KT_{\mathrm{s}}}\right)$, where $H_{n_{\mathrm{r}},n_{\mathrm{t}}}^{\mathrm{ow}}(f) = H_{n_{\mathrm{r}},n_{\mathrm{t}}}^{\mathrm{los}} + H_{n_{\mathrm{r}},n_{\mathrm{t}}}^{\mathrm{nlos}}(f)$ is the optical wireless channel transfer function at frequency f and T_{s} is the symbol period. $H_{n_{\mathrm{r}},n_{\mathrm{t}}}^{\mathrm{los}}$ is the line-of-sight (LoS) counterpart and $H_{n_{\mathrm{r}},n_{\mathrm{t}}}^{\mathrm{nlos}}(f)$ is the non-line-of-sight (NLoS) counterpart, respectively. The LoS channel is calculated by:

$$H_{n_{\mathrm{r}},n_{\mathrm{t}}}^{\mathrm{los}} = \frac{(m+1)\,A_{\mathrm{d}}\mathbf{1}_{\mathrm{v}}}{2\pi D_{n_{\mathrm{r}},n_{\mathrm{t}}}^2} \cos^m \phi_{n_{\mathrm{r}},n_{\mathrm{t}}} \cos\psi_{n_{\mathrm{r}},n_{\mathrm{t}}}, \qquad (2)$$

TABLE I
SPACE-DEPENDENT PARAMETERS

Parameters	Values
Room dimension [m]	$5 \times 5 \times 3$
Reflectivity of wall / ceiling	0.8
Reflectivity of floor	0.3
Half-power semiangle [degree]	$\phi_{1/2} = 60^\circ$
LED orientation	$\vec{o}_{n_{\mathrm{t}}} = [0, 0, -1]$
Detection area [cm^2]	$A_{\mathrm{pd}} = 0.25$
Field of view [degree]	$\psi_{\mathrm{FoV}} = 90^\circ$
UE 1 geometry:	$\vec{p}_{\mathrm{ue1}} = [0, 0, 0.75]$
	$\vec{o}_{\mathrm{ue1}} = [0.5, 0.5, 0.7071]$
UE 2 geometry:	$\vec{p}_{\mathrm{ue2}} = [1, 1.5, 0.75]$
	$\vec{o}_{\mathrm{ue2}} = [0.5, 0, 0.866]$

where m is the Lambertian emission order which is related to the half-power semiangle $\phi_{1/2}$ by $m = -1/\log_2(\cos\phi_{1/2})$; A_{d} is the detection physical area; $\mathbf{1}_{\mathrm{v}}$ refers to the LoS visibility function; $\phi_{n_{\mathrm{r}},n_{\mathrm{t}}}$, $\psi_{n_{\mathrm{r}},n_{\mathrm{t}}}$ and $D_{n_{\mathrm{r}},n_{\mathrm{t}}}$ are the light radiant angle, light incident angle and Euclidean distance. These three parameters are determined by the LED orientation $\vec{\mathbf{o}}_{n_{\mathrm{t}}}$ and location $\vec{\mathbf{p}}_{n_{\mathrm{t}}}$, PD orientation $\vec{\mathbf{o}}_{n_{\mathrm{r}}}$ and location $\vec{\mathbf{p}}_{n_{\mathrm{r}}}$. These vectors are illustrated in Fig. 2 (a).

Next, we use a simulation to explain the limitations in the scalability of SMP with regards to the number of LEDs and PDs. The simulation indoor environment is defined as a cubic room of size $5\ \mathrm{m} \times 5\ \mathrm{m} \times 3\ \mathrm{m}$, as shown in Fig. 2 (a). The N_{t} LEDs are deployed on the ceiling. The 2-dimensional (2-D) deployments of the LEDs with different number of LEDs are illustrated in Fig. 2 (b). Note that we try to distribute the LEDs uniformly to guarantee the coverage of the entire room and also to keep adequate distance between LEDs to lower the spatial correlation. On the receiver side, we consider using a smart phone type user equipment (UE) with a position of $\vec{p}_{\mathrm{ue}}$ and an orientation of $\vec{o}_{\mathrm{ue}}$. The deployment of PDs on the UE follows the multi-directional receiver (MDR) design presented in [7] as it offers a lower channel correlation. The dimension of the UE and the position $\vec{p}_{n_{\mathrm{r}}}$ / orientation $\vec{o}_{n_{\mathrm{r}}}$ of each PD relative to $\vec{p}_{\mathrm{ue}}$ and $\vec{o}_{\mathrm{ue}}$ with $N_{\mathrm{r}} = 16$ are illustrated in Fig. 2 (c). In the case of $N_{\mathrm{r}} < 16$, the PDs that shown in Fig. 2 (c) with numbering up to N_{r} are activated and the remaining PDs are deactivated. Two UEs with different locations and orientations are simulated. The total optical power is 18 dB and the number of subcarriers is $K = 256$. The NLoS channel transfer function is calculated using a FD method proposed in [8]. The remaining space-dependent

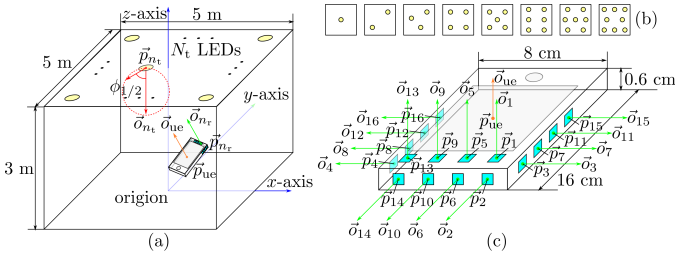

Fig. 2. (a) Optical wireless channel geometry. (b) 2-D geometric deployment with different number of LEDs from 1 to 8 in the simulation corresponding to Fig. 3. (c) Detailed geometric configuration of MDR.

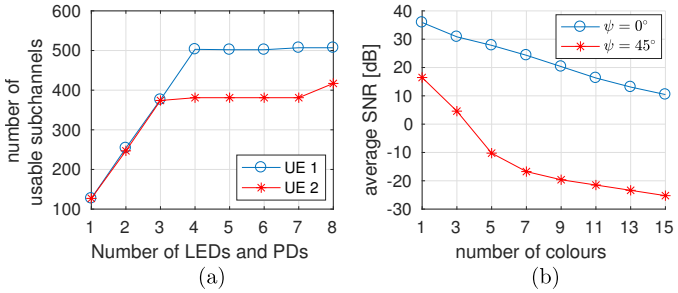

Fig. 3. (a) The number of usable subchannels varies with the number LEDs and PDs in a SMP system. Here the usable subchannel means the corresponding SNR is greater than 0 dB. (b) Average SNR over different multiplexing channels with $\psi = 0°, 45°$ in a WDM system.

parameters are listed in Table I. Note the factors other than space-dependent characteristics, such as low pass effects of frontends, are also considered in the simulation. However, we focus on the description of space-related properties in this section and the remaining factors will be presented in Section IV. In the simulation, the SNR of each subchannel is calculated using (1). In the ideal situation, there should be $I\tilde{K}$ subchannels in total. However, many subchannels have very low SNR and cannot be used for reliable transmission. Therefore, we count the number of subchannels that have a SNR greater than 0 dB as an indicator of usable subchannel. The results are shown in Fig. 3 (a). The number of usable subchannels scales linearly when the number of LEDs / PDs is not more than 3 for UE 1 and 4 for UE 2. However, the number of usable subchannels barely grows if the number of LEDs and PDs increases further. This is because of the strong spatial correlation which leads to the issue of channel matrix rank deficiency. Consequently, this issue limits the scalability of SMP systems in VLC.

III. Wavelength Division Multiplexing

WDM is another technique to realise parallel transmission as illustrated in Fig. 4 (a). We adopt the conventional OOK-WDM transmission model using C colours without precoding and post-processing [4]. Therefore, the transmitter and receiver are equipped with C coloured LEDs and C PDs with C different bandpass optical filters, respectively. Since we focus on the wavelength-dependent characteristics in this section, all LEDs and PDs are assumed to have the same position / orientation and NLoS channels are not included for simplicity. Therefore, the received signal by the n_{r}th PD is written as:

$$y_{n_{\mathrm{r}}}[n] = \sum_{n_{\mathrm{t}}=1}^{C} H^{\mathrm{los}}_{n_{\mathrm{r}},n_{\mathrm{t}}} H^{\lambda}_{n_{\mathrm{r}},n_{\mathrm{t}}} x_{n_{\mathrm{t}}}[n] + w_{n_{\mathrm{r}}}[n], \tag{3}$$

where $x_{n_{\mathrm{t}}}[n]$ is the transmitted signal from the n_{t}th LED with a variance of σ^2_{s}, $w_{n_{\mathrm{r}}}[n]$ is the noise samples detected by the n_{r}th PD with a variance of $\sigma^2_{\mathrm{w},n_{\mathrm{r}}}$ and the coefficient $H^{\lambda}_{n_{\mathrm{r}},n_{\mathrm{t}}}$ is defined as:

$$H^{\lambda}_{n_{\mathrm{r}},n_{\mathrm{t}}} = \int_{\lambda_{\min}}^{\lambda_{\max}} \mathcal{R}^{\mathrm{pd}}(\lambda)\mathcal{G}^{\mathrm{of}}_{n_{\mathrm{r}}}(\lambda)\mathcal{S}^{\mathrm{led}}_{n_{\mathrm{t}}}(\lambda)\mathrm{d}\lambda, \tag{4}$$

where $\mathcal{S}^{\mathrm{led}}_{n_{\mathrm{t}}}(\lambda)$ is the normalised spectral intensity, $\mathcal{G}^{\mathrm{of}}_{n_{\mathrm{r}}}(\lambda)$ is the optical filter spectral transmittance and $\mathcal{R}^{\mathrm{pd}}(\lambda)$ is the PD spectral responsivity. An analytical LED spectrum model is used for the calculation of $\mathcal{S}^{\mathrm{led}}_{n_{\mathrm{t}}}(\lambda)$ [4]:

$$\mathcal{S}^{\mathrm{led}}_{n_{\mathrm{t}}}(\lambda) = \frac{\exp\left(-\frac{(\lambda-\lambda_{0,n_{\mathrm{t}}})^2}{\Delta\lambda^2_{0.5}}\right) + 2\exp\left(-\frac{5(\lambda-\lambda_{0,n_{\mathrm{t}}})^2}{\Delta\lambda^2_{0.5}}\right)}{\Delta\lambda_{0.5}\left(\frac{\sqrt{\pi}}{2}+\sqrt{\frac{\pi}{5}}\right)\left(1+\mathrm{erf}\left(\frac{\lambda_{0,n_{\mathrm{t}}}}{\Delta\lambda_{0.5}}\right)\right)}, \tag{5}$$

where $\lambda_{0,n_{\mathrm{t}}}$ is the central frequency of the n_{t}th LED and $\Delta\lambda_{0.5}$ is a parameter determining the spectrum shape of the LED. This model has been demonstrated to be accurate compared to the off-the-shelf devices [4]. The optical filter can be modelled by a rectangular function:

$$\mathcal{G}^{\mathrm{of}}_{n_{\mathrm{r}}}(\lambda) = \begin{cases} G_{\mathrm{t}} & : \iota^{\mathrm{l}}_{n_{\mathrm{r}}} < \lambda < \iota^{\mathrm{r}}_{n_{\mathrm{r}}} \\ 0 & : \text{otherwise} \end{cases}, \tag{6}$$

where G_{t} is the filter transmittance, $\iota^{\mathrm{l}}_{n_{\mathrm{r}}}$ is left passband edge and $\iota^{\mathrm{r}}_{n_{\mathrm{r}}}$ is the right passband edge. Note that we keep the separate index notations for LEDs n_{t} and PDs n_{r}, because (3), (4), (5) and (6) will be used later in the description of HMP in Section IV. It has been pointed out in [5] that the passband of a thin-film optical filter shifts to shorter wavelengths with a light incident angle of $\psi > 0$. The passband wavelength shifting can be modelled by the following expression [5]:

$$\iota_{n_{\mathrm{r}}|\psi} = \iota_{n_{\mathrm{r}}|0^\circ}\sqrt{1-\sin^2\psi/\mathfrak{n}^2_{\mathrm{e}}}, \tag{7}$$

where $\mathfrak{n}_{\mathrm{e}}$ is the effective refraction index and $\iota_{n_{\mathrm{r}}|\psi}$ refers to the passband edge with incident angle ψ. This implies that $\mathcal{G}^{\mathrm{of}}_{n_{\mathrm{r}}}(\lambda)$ is also a function of ψ. This issue of bandpass shift is demonstrated in Fig. 4. With $\psi = 0°$, each optical filter matches the corresponding LED spectrum as expected. When ψ increases to $45°$, a considerable amount of spectrum mismatch can be observed. Since C colours are used in the WDM system, the spectrum central wavelength of an LED with cth colour is defined by

$$\lambda_0(c) = \lambda_{\min} + \frac{c-0.5}{C}(\lambda_{\max}-\lambda_{\min}), \tag{8}$$

for $c = 1, 2, \cdots, C$, which evenly distributes C LED spectra in the visible light spectrum of interest. The corresponding optical filter passband edge can be defined by $\iota^{\mathrm{l}}_{0^\circ}(c) = \lambda_0(c) - \Delta\iota/2$ and $\iota^{\mathrm{r}}_{0^\circ}(c) = \lambda_0(c) + \Delta\iota/2$ where $\Delta\iota$ is the width of the passband. Regarding the cth multiplexing channel, the signal

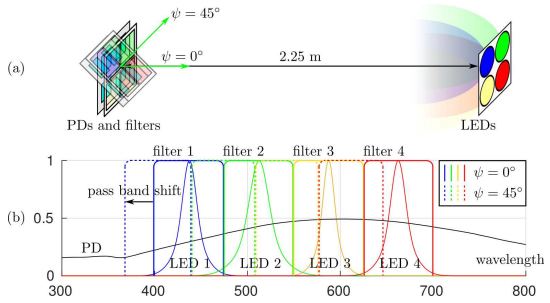

Fig. 4. (a) WDM system geometry with $\psi = 0°, 45°$. (b) Optical filter passband shift issue: it shows the relative LED spectral intensity, PD spectral responsivity and Optical filter passband with $\psi = 0°, 45°$.

from $(n_{\rm t} = c)$th LED is the desired signal and $\lambda_{0,n_{\rm t}=c} = \lambda_0(c)$. In addition, the $(n_{\rm r} = c)$th PD is decoded to extract the information and $\iota_{n_{\rm r}=c|0°} = \iota_{0°}(c)$. Therefore, the SNR on the cth multiplexing channel can be written as:

$$\gamma_c = \left(H^{\lambda}_{c,c}\right)^2 \left(\sum_{\hat{c}=1,\hat{c}\neq c}^{C} \left(H^{\lambda}_{c,\hat{c}}\right)^2 + \frac{\sigma^2_{{\rm w},c}}{\left(\sigma_{\rm s} H^{\rm los}\right)^2} \right)^{-1}. \quad (9)$$

Then we evaluate the scalability of a WDM system with the number of used colours C. Simulations with two different incident angles of $\psi = 0°, 45°$ are conducted. The link geometry is illustrated in Fig. 4 (a). To prevent excessive crosstalk, a passband width of $\Delta\iota = 15\ nm$ is used. An optical power of 18 dB is assumed. The PD spectral responsivity is plotted in Fig. 4 (b). The remaining wavelength dependent parameters are listed in Table II. The results of the average SNR over different multiplexing channel $\bar{\gamma} = 1/C \sum_{c=1}^{C} \gamma_c$ are shown in Fig. 3 (b). It can been seen that by increasing the number of used colours, the spectrum separation between the LEDs of different colour becomes narrower. With a limited range of visible light spectrum (400-700 nm) and a fixed spectrum width of each coloured LED (tens of nm), crosstalk between subchannels of different colours will increase and will eventually become the limiting factor. Consequently, the average SNR decreases with the number of used colours. Furthermore, it can be observed that the SNR drops significantly due to the colour mismatch when the receiver is tilted by $45°$ especially when C is large. Therefore, the scalability of a WDM system will be limited by crosstalk when too many colours are used and it is vulnerable to the passband shift caused by non-zero incident angle.

IV. Hybrid Multiplexing

The concept of MIMO techniques are originally proposed to explore the DoF in SD. Later in the field of VLC, the concept of colour-MIMO has been proposed to more efficiently explore DoF in WD [5]. Here we propose a hybrid MIMO system which explores the DoF in both SD and WD jointly. On the one hand, the DoF in WD has the potential to decorrelate the channels where spatial correlation is strong. On the other hand, with precoding and post-processing techniques that are designed for conventional MIMO systems, the crosstalk in WDM-VLC systems can be effectively mitigated. Thus, a well-conditioned channel matrix is expected from this hybrid MIMO system and thereby achieving an improved multiplexing capability. This is the main idea of the HMP. In order to include the space-dependent and wavelength dependent characteristics into the hybrid MIMO system, the relationship between the space and wavelength dependent parameters and the hybrid MIMO channel matrix is required. Therefore, we establish a framework for the hybrid MIMO system in the context of the MIMO-OFDM model presented in Section II in the following subsection.

TABLE II
Wavelength Dependent Parameters

Parameters	Values
Wavelength range [nm]	$[\lambda_{\min} = 400, \lambda_{\max} = 700]$
Optical filter effective refractive index	$\mathfrak{n}_{\rm e} = 1.83$
Optical filter transmittance	$G_{\rm t} = 1$

A. A hybrid MIMO channel matrix framework

Here we reuse the MIMO-OFDM model shown in Fig. 1. The blocks before $x_{n_{\rm t}}[n]$ and after $y_{n_{\rm r}}[n]$ are the same as those of conventional SMP systems, where $x_{n_{\rm t}}[n]$ is the discrete-time transmitted signal for the $n_{\rm t}$th LED and $y_{n_{\rm r}}[n]$ is the discrete-time received signal from the $n_{\rm r}$th PD. All of the space and wavelength dependent characteristics are embedded in the process between $x_{n_{\rm t}}[n]$ and $y_{n_{\rm r}}[n]$ and this is the interest of this framework. Starting from $x_{n_{\rm t}}[n]$, the bipolar discrete signal experiences scaling, addition of DC-bias, and pulse shaping before it is forwarded to the $n_{\rm t}$th LED:

$$x_{n_{\rm t}}(t) = \sum_{n=-\infty}^{\infty} (\sigma_{\rm x} x_{n_{\rm t}}[n] + 1) g(t - nT_{\rm s}), \quad (10)$$

where $\sigma_{\rm x}$ is a scaling factor and $g(t)$ is a band-limited pulse shaping function. The root-square raised cosine (RRC) function is defined for $g(t)$ in this study. The following series of process via LEDs, optical wireless channels and PDs can be described by the following expression:

$$i_{n_{\rm r}}(t) = \int_{\lambda_{\min}}^{\lambda_{\max}} \overbrace{\left\{\mathcal{R}^{\rm pd}(\lambda)\mathcal{G}^{\rm of}_{n_{\rm r}}(\lambda)h^{\rm pd}(t)\right\}}^{\text{PD \& optical filter}} * \overbrace{h^{\rm ow}_{n_{\rm r},n_{\rm t}}(t)}^{\text{optical wirelss}} * \underbrace{\left\{\bar{p}_{n_{\rm t}}\mathcal{S}^{\rm led}_{n_{\rm t}}(\lambda)h^{\rm led}(t)\right\}}_{\text{LED}} * \underbrace{x_{n_{\rm t}}(t)}_{\text{signal}} {\rm d}\lambda, \quad (11)$$

where $i_{n_{\rm r}}(t)$ is the photocurrent from the $n_{\rm r}$th PD, $*$ is the convolution operator, $\bar{p}_{n_{\rm t}}$ is the optical power of the $n_{\rm t}$th LED, $h^{\rm pd}(t)$ and $h^{\rm led}(t)$ are the low pass impulse response of the LED and PD, respectively. $h^{\rm ow}_{n_{\rm r},n_{\rm t}}(t)$ is the impulse response of optical wireless channel and the corresponding Fourier transform equals $H^{\rm ow}_{n_{\rm r},n_{\rm t}}(f)$. Finally, the photocurrent is forwarded to a matched filter. By correlating with the $g(t)$ and sampling at $nT_{\rm s}$, the discrete time received signal is $y_{n_{\rm r}}[n] = \{i_{n_{\rm r}} * g\}(nT_{\rm s})$. The equivalent overall channel impulse response before sampling is calculated by its definition

TABLE III
HMP PARAMETER CONFIGURATIONS

	LED position vectors [m]			LED central wavelength [nm]			filter passband centre/width [nm]		
index	config1	config2	config3	config1	config2	config3	config1	config2	config3
1	$[-1.875, -1.875, 3]$	$[-0.0375, -0.0375, 3]$	$[-1.275, -1.275, 3]$	450	409	438	470/140	422/43	451/103
2	$[-1.875, -0.625, 3]$	$[-0.0375, -0.0125, 3]$	$[-1.275, -1.225, 3]$	450	428	513	470/140	441/44	451/103
3	$[-1.875, 0.625, 3]$	$[-0.0375, 0.0125, 3]$	$[-1.225, -1.275, 3]$	450	447	588	470/140	460/45	451/103
4	$[-1.875, 1.875, 3]$	$[-0.0375, 0.0375, 3]$	$[-1.225, -1.225, 3]$	450	466	663	470/140	479/46	451/103
5	$[-0.625, -1.875, 3]$	$[-0.0125, -0.0375, 3]$	$[-1.275, 1.225, 3]$	450	484	438	470/140	499/47	529/107
6	$[-0.625, -0.625, 3]$	$[-0.0125, -0.0125, 3]$	$[-1.275, 1.275, 3]$	450	503	513	470/140	518/49	529/107
7	$[-0.625, 0.625, 3]$	$[-0.0125, 0.0125, 3]$	$[-1.225, 1.225, 3]$	450	522	588	470/140	537/50	529/107
8	$[-0.625, 1.875, 3]$	$[-0.0125, 0.0375, 3]$	$[-1.225, 1.275, 3]$	450	541	663	470/140	557/51	529/107
9	$[0.625, -1.875, 3]$	$[0.0125, -0.0375, 3]$	$[1.225, -1.275, 3]$	450	559	438	470/140	576/52	606/111
10	$[0.625, -0.625, 3]$	$[0.0125, -0.0125, 3]$	$[1.225, -1.225, 3]$	450	578	513	470/140	595/53	606/111
11	$[0.625, 0.625, 3]$	$[0.0125, 0.0125, 3]$	$[1.275, -1.275, 3]$	450	597	588	470/140	615/54	606/111
12	$[0.625, 1.875, 3]$	$[0.0125, 0.0375, 3]$	$[1.275, -1.225, 3]$	450	616	663	470/140	634/55	606/111
13	$[1.875, -1.875, 3]$	$[0.0375, -0.0375, 3]$	$[1.225, 1.225, 3]$	450	634	438	470/140	653/56	683/116
14	$[1.875, -0.625, 3]$	$[0.0375, -0.0125, 3]$	$[1.225, 1.275, 3]$	450	653	513	470/140	672/57	683/116
15	$[1.875, 0.625, 3]$	$[0.0375, 0.0125, 3]$	$[1.275, 1.225, 3]$	450	672	588	470/140	692/58	683/116
16	$[1.875, 1.875, 3]$	$[0.0375, 0.0375, 3]$	$[1.275, 1.275, 3]$	450	691	663	470/140	711/59	683/116

as: $h_{n_\mathrm{r},n_\mathrm{t}}(t) = \{i_{n_\mathrm{r}} * g\}(t|x_{n_\mathrm{t}}[n] = \delta[n])$. In conjunction with (4), (10) and (11), the channel frequency response equals the fast Fourier transform (FFT) of $h_{n_\mathrm{r},n_\mathrm{t}}(t)$ as:

$$H_{n_\mathrm{r},n_\mathrm{t}}(f) = H^{\lambda}_{n_\mathrm{r},n_\mathrm{t}} H^{\mathrm{ow}}_{n_\mathrm{r},n_\mathrm{t}}(f) \times \bar{p}_{n_\mathrm{t}} H^{\mathrm{led}}(f) H^{\mathrm{pd}}(f) G^2(f)(\sigma_\mathrm{x} + \delta(f)), \quad (12)$$

where $H^{\mathrm{led}}(f)$, $H^{\mathrm{led}}(f)$ and $G(f)$ are the Fourier transform of $h^{\mathrm{led}}(t)$, $h^{\mathrm{led}}(t)$ and $g(t)$, respectively. Based on the definition of discrete time Fourier transform (DTFT), the channel transfer function after the sampling at nT_s is a periodic summation of $H_{n_\mathrm{r},n_\mathrm{t}}(f)$ with a period of $1/T_\mathrm{s}$ as: $H^{1/T_\mathrm{s}}_{n_\mathrm{r},n_\mathrm{t}}(f) = \sum_{l=-\infty}^{\infty} H_{n_\mathrm{r},n_\mathrm{t}}(f - l/T_\mathrm{s})$ Thus the channel transfer function between the n_tth LED and the n_rth PD on the kth subcarrier can be calculated as: $[\mathbf{H}_k]_{n_\mathrm{r},n_\mathrm{t}} = H^{1/T_\mathrm{s}}_{n_\mathrm{r},n_\mathrm{t}}(k/KT_\mathrm{s})$, for $k = 0, 1, \cdots, K-1$. Up to now, the hybrid MIMO framework is complete. With this framework, a hybrid MIMO matrix can be obtain based a large number of space and wavelength dependent parameters.

B. Configuration to parameters in SD and WD

The significance of hybrid MIMO is that it increases the DoF of the MIMO system. In order to utilise the extra DoF, appropriate configuration to space and wavelength dependent parameters should be used. Note that the selection of parameters should take the practical constraints into account. For example, $\phi_{1/2}$ has to be large enough to guarantee the lighting performance and the coverage of each LED. Some parameters are determined by the random factors, such as the orientation and location or UE. Due to the large quantity of parameters, it is challenging to find an optimal configuration with the limited space in this paper. Therefore, three example configurations are considered to demonstrate the potential of the HMP system to improve the multiplexing capability. In a future work an algorithm will be proposed for optimizing the configuration. The configurations are under the same indoor environment illustrated in Fig. 2 (a) with $N_\mathrm{t} = 16$. In addition, the same UE illustrated in 2 (c) is also used with $N_\mathrm{r} = 16$. The common space and wavelength dependent parameters specified in Table I and II are also used here. The major geometry and wavelength dependent parameters are listed in Table III.

1) Configuration 1: Only the DoF in SD is utilised. LEDs are spatially separated and only one colour is used. This is equivalent to a SMP system.

2) Configuration 2: Only the DoF in WD is utilised. Each pair of LED and PD uses a different colour. All LEDs are gathered in the centre of the room. This is equivalent to a WDM system with precoding and post-processing to suppress the inter-colour crosstalk.

3) Configuration 3: The DoFs in both SD and WD are utilised. Every four LEDs are clustered at each quadrant of the room. Four colours are used in total. LEDs in the same cluster use spectra of different colours. In addition, PDs on the same side of the UE uses optical filters of different colours.

Note that the passband of the optical filter in a conventional WDM system is typically limited to a narrow range around the central wavelength of the corresponding LED spectrum. In contrast, thanks to the crosstalk mitigation capability, the optical filter passband in HMP can be broadened. In addition, the filter centre wavelength is slightly extended to the right to compensate for the passband shift issue.

V. SIMULATION RESULTS

In this section, we present the simulation results of the system using the configuration specified in Section IV-B. The signal scaling factor is $\sigma_\mathrm{x} = 0.3125$. Firstly, we calculate the SNR of each subchannel based on (1) of systems with a total optical power of 18 dB of UE 1. The histogram of the SNRs are shown in Fig 5 (a). With a $I = 16$ and $K = 256$, the total number of potential multiplexing subchannels is 2032. In the subplot of Fig. 5 (a), we can see that configurations 1 and 2 have only 508 and 825 subchannels with an SNR exceeding 0 dB, respectively. In contrast, this number is 1756 for configuration 3. This demonstrates that by using the characteristics in both SD and WD, a better conditioned channel matrix can be obtained and a greater number of eigen-subchannels can be established. Next, we

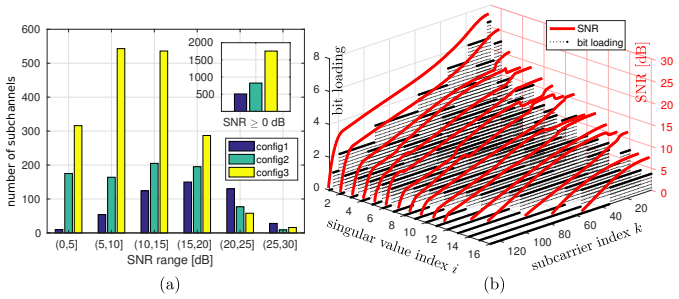

Fig. 5. (a) SNR histogram of HMP systems with various configurations. (b) Bit-loading in HMP system with configuration 3 and optical power of 18 dB.

compare the bit error rate (BER) performance of HMP with various configurations. In this simulation, an adaptive bit loading method presented in [9] is used (Section II steps 1 to 9). This loading algorithm minimises the BER with a specified data rate. An example of a bit loading solution is demonstrated in Fig. 5 (b). Transmission data rates of 500 Mbps, 1 Gbps and 1.5 Gbps are considered with a single side modulation bandwidth of $1/(2T_{\mathrm{s}}) = 50$ MHz. In addition to the link level simulations, analytical calculation results using (18) in [10] are also provided for comparison. The BER results are shown in Fig. 6. For the data rate of 500 Mbps, the HMP systems with all three configurations are able to achieve a BER lower than 1×10^{-3} with optical power in the range between 15 to 20 dB. This is because the required number of usable subchannels is relatively small. With extra subchannels available, the HMP system with configuration 3 is able to achieve the lowest BER by loading fewer numbers of bits to more subchannels. When the data rate increases to 1 and 1.5 Gbps, the numbers of subchannels of configuration 1 and 2 are no longer sufficient. Therefore, the loading algorithm has to load a greater number to bits to each subchannel in order to fulfil the data rate requirement. Consequently, this leads to an excessive BER of more than 5×10^{-2} with a high optical power of 20 dB. In contrast, the system with configuration 3 is still able to achieve a BER of 1×10^{-3} with a data rate of 1.5 Gbps with the same amount of optical power. Comparing the performance of UE 1 and 2, the performance of UE 2 is worse than that of UE 1. This is because the position of UE 2 is away from the room centre and experiences a slightly worse channel. However, the BER degradation in configuration 3 is minimal compared to the other two configurations. These results demonstrate the potential of HMP with configuration 3. A general rule of thumb for configuration 3 can be concluded as: use WD to decorrelate the LEDs or PDs that are strongly correlated in SD.

VI. Conclusions

In this paper, a hybrid MIMO multiplexing OFDM-based VLC system is proposed. A general framework for a hybrid MIMO system that depends on space and wavelength dependent characteristics is established. Based on this framework, we evaluate the performance of HMP systems with three different configurations and demonstrate that HMP has the potential to significantly increase the number of multiplexing channels, thereby supporting higher data rates.

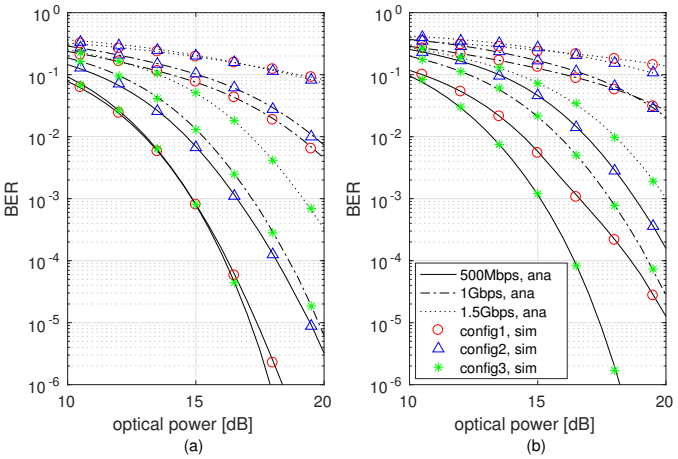

Fig. 6. BER against total optical power for UE 1 (a) and UE 2 (b). 'sim': simulation results. 'ana': analytical results.

Acknowledgement

The authors gratefully acknowledge the support of this research by the Engineering and Physical Sciences Research Council (EPSRC) grant EP/L020009/1: Towards Ultimate Convergence of All Networks (TOUCAN). Professor Haas acknowledges the financial support from the Wolfson Foundation, the EPSRC UK under Established Career Fellowship grant EP/R007101/1.

References

[1] H. Haas, L. Yin, Y. Wang, and C. Chen, "What is LiFi?" *J. Lightw. Technol.*, vol. 34, no. 6, pp. 1533–1544, Mar. 2016.

[2] R. Bian, I. Tavakkolnia, and H. Haas, "15.73 Gb/s Visible Light Communication With Off-the-Shelf LEDs," *J. Lightw. Technol.*, vol. 37, no. 10, pp. 2418–2424, May 2019.

[3] Y. Hong, T. Wu, and L. Chen, "On the Performance of Adaptive MIMO-OFDM Indoor Visible Light Communications," *IEEE Photonics Technol. Lett.*, vol. 28, no. 8, pp. 907–910, Apr. 2016.

[4] L. Cui, Y. Tang, H. Jia, J. Luo, and B. Gnade, "Analysis of the Multichannel WDM-VLC Communication System," *J. Lightw. Technol.*, vol. 34, no. 24, pp. 5627–5634, Dec. 2016.

[5] P. Ge, X. Liang, J. Wang, C. Zhao, X. Gao, and Z. Ding, "Optical Filter Designs for Multi-Color Visible Light Communication," *IEEE Trans. Commun.*, vol. 67, no. 3, pp. 2173–2187, Mar. 2019.

[6] Y. Xiao, Y.-J. Zhu, and Z.-G. Sun, "Linear Precoding Designs for MIMO VLC Using Multi-Color LEDs under Multiple Lighting Constraints," *Crystals*, vol. 8, no. 11, 2018.

[7] M. D. Soltani, M. A. Arfaoui, I. Tavakkolnia, A. Ghrayeb, M. Safari, C. M. Assi, M. O. Hasna, and H. Haas, "Bidirectional Optical Spatial Modulation for Mobile Users: Toward a Practical Design for LiFi Systems," *IEEE J. Sel. Areas Commun.*, vol. 37, no. 9, pp. 2069–2086, Sep. 2019.

[8] H. Schulze, "Frequency-Domain Simulation of the Indoor Wireless Optical Communication Channel," *IEEE Trans. Commun.*, vol. 64, no. 6, pp. 2551–2562, June 2016.

[9] P. S. Chow, J. M. Cioffi, and J. A. C. Bingham, "A Practical Discrete Multitone Transceiver Loading Algorithm for Data Transmission over Spectrally Shaped Channels," *IEEE Trans. Commun.*, vol. 43, no. 2/3/4, pp. 773–775, Feb. 1995.

[10] Jianhua Lu, K. B. Letaief, J. C. . Chuang, and M. L. Liou, "M-PSK and M-QAM BER Computation using Signal-Space Concepts," *IEEE Trans. Commun.*, vol. 47, no. 2, pp. 181–184, Feb. 1999.